Engineering Structures 274 (2023) 115070

Contents lists available at ScienceDirect

Engineering Structures

journal homepage: www.elsevier.com/locate/engstruct

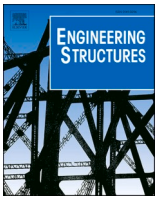

Experimental investigation of the influence of the timing of strengthening on the structural behavior of segmental tunnel linings

Xian Liu [a,b], Zijie Jiang [a], Herbert A. Mang [c,*]

[a] College of Civil Engineering, Tongji University, Shanghai, China
[b] Key Laboratory of Performance Evolution and Control for Engineering Structures, Ministry of Education, Tongji University, Shanghai, China
[c] Institute for Mechanics of Materials and Structures, Vienna University of Technology, Vienna, Austria

ARTICLE INFO

Keywords:
Strengthening of shield tunnels
Timing of strengthening
Full-scale test
Composite structure

ABSTRACT

If the serviceability of an existing shield tunnel structure is endangered, strengthening is required. A newly proposed technique of strengthening of segmental tunnel linings, called *steel plate – concrete composite structure (SPCCS)* strengthening, was experimentally investigated in previous research, in which the tunnel lining was strengthened at the ultimate state. Such a strengthening scheme is denoted as *delayed strengthening*. Experimental results have shown that the new strengthening technique is advantageous in enhancing the design life of shield tunnels, as compared to traditional strengthening techniques. However, in engineering practice, the tunnel lining must be strengthened before the ultimate state is reached. Hence, the timing of strengthening is a critical parameter in the design of the strengthening process. In the present research, a full-scale test was conducted such that the segmental tunnel lining was strengthened *ab initio*, i.e. before being subjected to external loading. This mode of strengthening is termed as *initial strengthening scheme*. The ultimate capacity, the failure process, and the failure mode were investigated. The failure mechanism, the ultimate capacity, the ductility, and the toughness of segmental tunnel linings, reinforced by the SPCCS strengthening technique, were compared with the ones of initial and delayed strengthening schemes. It is shown that the timing of strengthening does not have much influence on the ultimate capacity. However, it has a significant influence on the stiffness, the ductility, and the toughness. The ultimate load bearing capacity of the strengthened structure in case of initial strengthening was found to be only 5.7 % larger than the one in case of delayed strengthening, whereas the increase of the structural stiffness, the ductility, and the toughness is 520.6 %, 46.1 %, and 64.6 %, respectively. Regarding the utilization efficiency of the steel plate, the results have shown that the earlier the structure is strengthened, the greater the utilization efficiency of the strengthening material.

1. Introduction

The shield tunneling method is mechanically effective and environmentally friendly. For these reasons, shield tunnels are widely used in underground metro systems. The most common form of the cross-section of shield tunnels is the one of circular segments. An advantage of the structural behavior of circular segmental tunnel linings is the arching effect. However, these linings are sensitive to the overburden of the vertical load and the reduction of the horizontal load [4]. Unfavorable environmental conditions may result in serviceability problems such as water ingress through the lining into the tunnel [9], cracking of concrete [22,1], the opening of segmental joints [6], and even structural failure. Strengthening is required when the structural serviceability or the safety of the structure are endangered.

A new strengthening technique, called *steel plate – concrete composite structure (SPCCS)* strengthening technique, as shown in Fig. 1, was recently proposed [13]. Compared to the traditional *epoxy-bonded steel plate (EBSP)* strengthening technique, which is presently the most widely used strengthening technique on a world-wide scale [8,11], epoxy is replaced by a combination of studs, embedded steel bars, adhesive anchors, and steel-fiber reinforced concrete to establish the bond between the strengthening material and the segmental tunnel lining. An experimental investigation was carried out on a deformed segmental tunnel lining, reinforced by the SPCCS strengthening technique. It was shown that the failure mode for this strengthening technique is more ductile than the one for the EBSP strengthening technique. Additionally,

* Corresponding author.
E-mail addresses: xian.liu@tongji.edu.cn (X. Liu), jzj055880@tongji.edu.cn (Z. Jiang), herbert.mang@tuwien.ac.at (H.A. Mang).

https://doi.org/10.1016/j.engstruct.2022.115070
Received 10 February 2022; Received in revised form 30 June 2022; Accepted 1 October 2022
Available online 26 October 2022

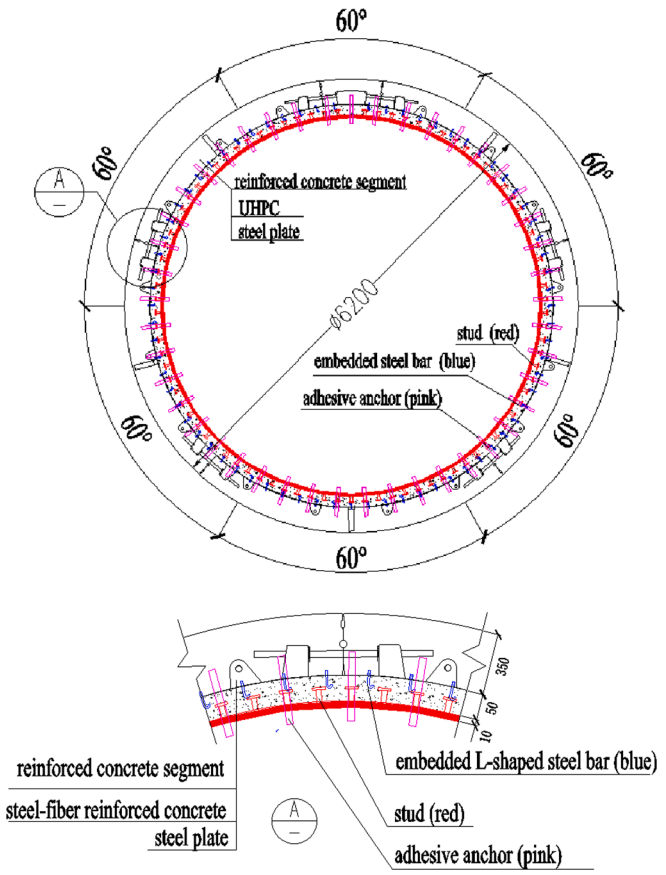

Fig. 1. Cross-section of the investigated structure (unit: mm), reinforced by the SPCCS strengthening technique.

the advantages of the SPCCS strengthening technique are greater than the ones of the EBSP strengthening technique. Not least, the amount of steel in the former is significantly smaller than the one in the latter [13]. In previous research, the segmental lining, reinforced by the SPCCS strengthening technique, was investigated experimentally with a delayed strengthening scheme [13]. In this loading scheme, the structure was strengthened when the unstrengthened structure had reached the ultimate state. This loading scheme was employed to investigate the mechanical behavior of segmental tunnel linings strengthened by different techniques, such as the *epoxy-bonded filament wound profiles (EBFWP)* strengthening technique [10] and the EBSP strengthening technique [11].

However, in engineering practice, it is inconvenient and even dangerous to strengthen the tunnel lining at the ultimate state. The tunnel should be strengthened earlier to avoid hazards. The proper timing of strengthening of tunnels is very important. However, so far this item has not been investigated thoroughly and discussed in sufficient detail in the literature. On the other hand, the SPCCS strengthening technique has been discussed intensively for the cases of initial strengthening of beams and frames, where the structure is reinforced before being subjected to external loads. Static loading tests were conducted on SPCC beams to investigate the mechanical behavior in case of bending [16,19], transverse shear [17], and of a combination of bending and torsion [18]. Mechanical models were established on the basis of the theory of elasticity [19]. Equations for the calculation of the strength of SPCC beams were derived [16,17]. Besides, a series of tests on SPCC frames was performed [3], and an experimental investigation was carried out on a two-story SPCC frame [15]. These tests provided the basis for the development and the use of analysis models [20]. However, no literature was found regarding tunnels initially strengthened by the SPCCS technique. This was the motivation for carrying out a full-scale test based on initial strengthening.

The purpose of this paper is to report on the load-carrying mechanism and the failure process. The failure mechanism, the ultimate capacity, the ductility, and the toughness of segmental tunnel linings, initially reinforced by the SPCCS technique, were compared with the corresponding quantities in case of delayed strengthening schemes. The full-scale test, with an identical structural configuration including dimensions and material properties, but with a different strengthening scheme compared to the one in the test conducted by Liu et al. [13], is the basis of this research. The results from this test series are subsequently compared. This research is a necessary prerequisite for the development and the use of analysis models considering the influence of the timing of strengthening.

2. Experimental program

2.1. SPCCS strengthening technique

The SPCCS strengthening technique was introduced in detail in previous research [13]. Fig. 1 shows the cross-section of the investigated structure, reinforced by this technique. The bond between the steel plate and the concrete segment is established by a combination of struts, welded to the surface of the steel plate, L-shaped steel bars, embedded into the inner surface of the segmental tunnel lining (old concrete), adhesive anchors, providing radial force resistance of the bond, and steel-fiber reinforced concrete (new concrete). Struts are shear connectors between the steel plate and the new concrete. L-shaped steel bars are shear connectors between the old and the new concrete. Adhesive anchors are pull-out connectors between the steel plate and the old concrete. Steel-fiber reinforced concrete of high crack resistance is used to fill the gap between the steel plate and the old concrete to bond the connectors together.

2.2. Experimental specimen

One full ring is tested in this study. The parameters of the experimental specimen are the same as the ones in previous research [13], listed in Table 1. Unstrengthened segmental tunnel linings are widely used in the Shanghai rail transit. Such a lining is shown in Fig. 2. It consists of six segments, named F, L1, L2, B1, B2, and D. The outer and the inner diameter of the structure are 6200 mm and 5500 mm, respectively. Bolts are used at the segmental joints to connect adjacent segments. The six segmental joints are located at 8°, 73°, 138°, 222°, 287°, and 352°. The thickness and the width of the steel plate are 10 mm and 1200 mm, respectively.

2.3. Loading system and loading process

The self-balanced horizontal loading system and the friction reduction system are shown in Fig. 3. The self-balanced horizontal loading

Table 1
Material parameters.

Material type	Dimensions	Young's modulus [N/mm^2]	Compressive strength [N/mm^2]	Yield strength [N/mm^2]
Old concrete	350 mm × 1200 mm	3.13×10^4	67.43	—
Bolt	30 mm (diameter)	2.03×10^5	—	454.85
New concrete	50 mm × 1200 mm	3.13×10^4	67.43	—
Steel plate	10 mm × 1200 mm	1.70×10^5	—	238.22
Embedded steel bars	—	2.02×10^5	—	281.67

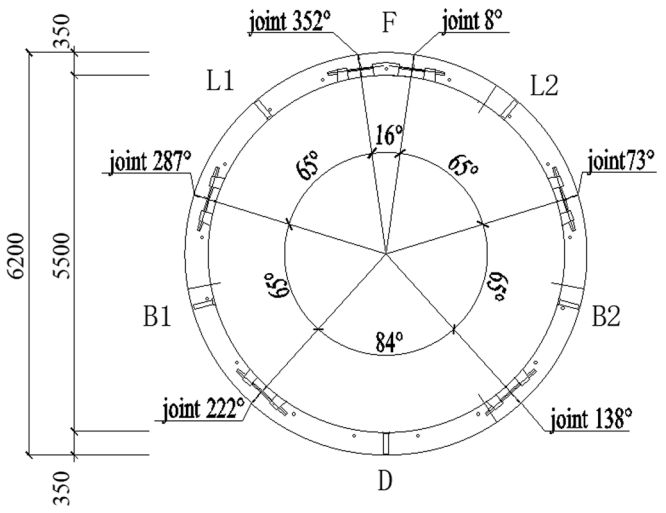

Fig. 2. Cross-section of the unstrengthened segmental tunnel lining (unit: mm).

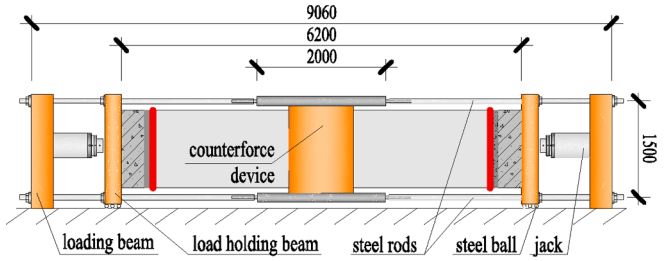

Fig. 3. Profile diagram of the self-balanced horizontal loading system (unit: mm).

system contains 24 load points. The axis of each point load is passing through the center of the system. The friction reduction system contains 192 steel balls between the specimen and the ground.

As shown in Fig. 4(a), 24 point loads are divided into three groups, i. e. six forces P1, ten forces P2, and eight forces P3. P1, P2, and P3 simulate the vertical earth pressure, the horizontal earth pressure, and the load on the shoulder of the structure, respectively. The loading scheme in the test is shown in Fig. 4(b). It consists of two stages. In stage 1, P1, P2, and P3 are increasing simultaneously, noting that P2 = 0.65 × P1, where 0.65 is the value of the lateral earth pressure coefficient in Shanghai, and P3 = 0.5 × (P1 + P2), which results in a smooth distribution of the external loading from the P1 zone to the P2 zone. Stage 2 starts when P2 reaches the value of the passive earth pressure. It is determined by the soil properties in Shanghai. In this stage, P2 is kept constant while P1 is increasing continuously, noting that P3 = 0.5 × (P1 + P2). Stage 2 ends when the structure fails. The loading system is identical to that in previous research [13], but the loading process is different. In that research, the unstrengthened structure was loaded up to a vertical convergence of 120 mm. Afterwards, the structure was strengthened and the test was continued until the structure failed. The main difference between these two loading schemes is the timing of strengthening. In the former scheme, the structure is strengthened initially, whereas in the latter, it is strengthened just before reaching the ultimate state.

The design of the loading process is based on the following considerations: (1) The distribution of the loads acting on the tested lining is similar to the real external loading of segmental linings in engineering practice. (2) The internal forces (bending moments and axial forces) of critical cross-sections are equal to those in real tunnel structures. Numerous numerical simulations were carried out to ensure this. (3) This design strategy was employed in tests, on the structural level, for

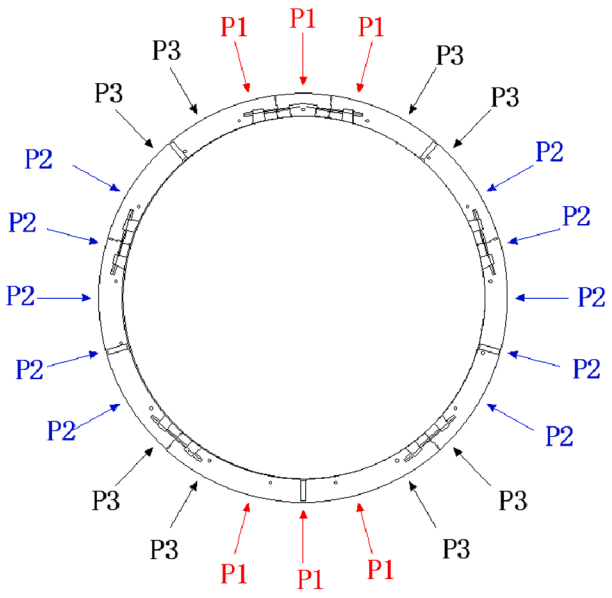

(a)

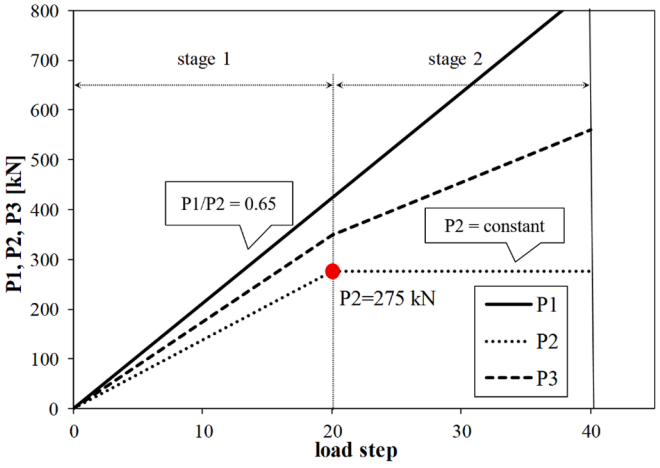

(b)

Fig. 4. (a) Distribution of point loads; (b) loading scheme.

segmental linings [21,2,14,13].

2.4. Measurement program

During the test, the structural deformations, the dilations of the segmental joints, the strains of the steel reinforcement, of the concrete, the bolts, and of the steel plate, furthermore, the relative tangential slippage and the radial stripping value between different material layers are monitored. Information on the corresponding measurement device is listed in Table 2.

The above mentioned items are measured in this test to determine the deformation of the structure and the internal forces during the loading process. Joint dilations are measured because they contribute, to a considerable amount, to the total structural deformation. The strains of each layer of material are measured to calculate the internal forces on key cross-sections. The relative displacements between different material layers are monitored to assess the bond behavior of the strengthened structure.

Table 2
Information on measurement points.

Test item	Sensor	Model	Range	Precision	Number
Overall deformation	Displacement meter	LVDT	500 mm	0.01 mm	14
Strain of steel reinforcing	Strain gauge	BX120-3AA	20,000με	1με	136
Strain of bolt	Strain gauge	JTM-Y1800	20,000με	1με	12
Strain of concrete	Strain gauge	DX50AA-120	20,000με	1με	136
Joint dilation	Displacement meter	LVDT	100 mm	0.01 mm	24
Strain of steel plate	Strain gauge	BX120-3AA	20,000με	1με	128
Relative slippage	Displacement meter	LVDT	100 mm	0.01 mm	24
Relative stripping value	Displacement meter	LVDT	100 mm	0.01 mm	24

3. Experimental results

The load – vertical convergence diagram from the test with initial strengthening is shown in Fig. 5. In the following, the failure process will be described: (1) the outer concrete cracked at 270°; (2) the steel plate yielded at 180°; (3) the core concrete zone cracked in compression at joint 8° and the steel plate yielded at 15°; (4) the steel plate yielded in the region from 352° to 0°; (5) the steel plate yielded in the region from 345° to 8° and the bolt yielded at joint 287°; (6) the steel plate yielded in the region from 180° to 195°, and at 287°, and the bolt yielded at joint 73°; (7) the core concrete zone cracked in compression at joint 352°, and the outer concrete crushed at joint 8°; (8) the steel reinforcement yielded at 180°; (9) bond failure occurred at the top and at the bottom of the structure, the bolts at 73° and 287° failed in tension, and the outer concrete crushed at joints 352°, 180°, and 195°.

3.1. Structural state at failure

The structure failed at P1 = 821 kN. The state of the structure at failure is shown in Fig. 6. The outer concrete at joints 8° and 352° crushed in compression. The outer concrete of the segment at 180° and 195° crushed in compression. The bolts at joints 73° and 287° failed in tension. The tensile stress of the steel plate reached the yield stress in the regions ranging from 345° to 15° and from 180° to 195°. The compressive stress reached the yield stress at 287°. The bond between the old and the new concrete failed in the regions ranging from 320° to 28° and from 150° to 230°.

3.1.1. Segment failure

Segment failure consists of cracking in tension and crushing in compression. The first crack occurred at P1 = 506 kN on the outer surface of the structure at 270°. The crack width was 0.02 mm. Crack propagation started at P1 = 546 kN on the outer surface at 270°, as shown in Fig. 7(a). The maximum width of these cracks was 0.05 mm.

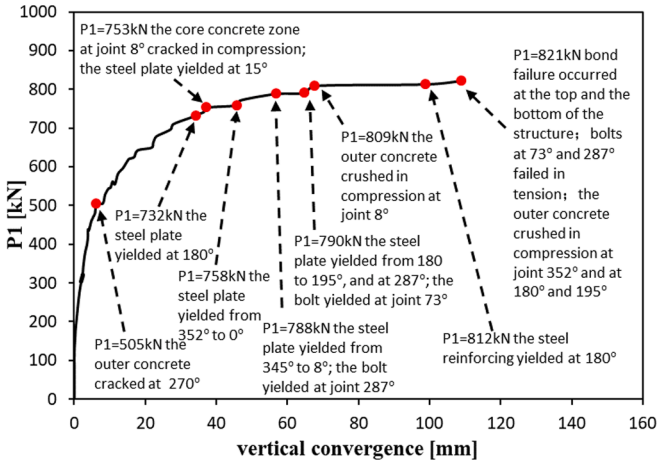

Fig. 5. Load – vertical convergence diagram of a segmental tunnel lining, strengthened by the SPCCS technique.

With increasing load, more cracks occurred in the regions around 90° and 270°. At the load level P1 = 809 kN, the crack distance at 90° and 270° was 200 mm; the maximum crack width was 0.1 mm. When P1 reached 821kN, the outer concrete at 180° and 195° crushed in compression. The distribution of the cracks around 90° and 270° is shown in Fig. 7(b) and Fig. 7(c), respectively. Concrete crushing at the failure state, i.e. at P1 = 821 kN, at 180° and 195°, is illustrated in Fig. 7 (d). Regions of segment failure are shown in Fig. 7(e), where the black solid lines represent the cracks, and the shading indicates failure in compression. The cracks on the inner surface of the segmental tunnel lining could not be inspected because they were hidden by the steel plate and the new concrete. The inner surface cracks are insignificant, because the steel plate and the new concrete prevent durability problems caused by these cracks.

3.1.2. Joint damage

The segmental joints represent discontinuities of the tunnel lining. The six joints are subjected to combinations of an axial force and a bending moment. In the test, negative bending moments occurred at joints 73° and 287°, where the outer part of the joint opened and its inner part was closed. Positive bending moments, however, occurred at the remaining four joints, where the inner part of the joint opened and its outer part was closed. Fig. 8 shows all joints after the strengthened structure has reached the failure state. The outer concrete at joints 8° and 352° was crushed and spalled. Splitting in form of compression cracks of the inner concrete occurred at joints 73° and 287°. Joints 138° and 222° remained intact. It is noteworthy that the bolts at joints 73° and 287° failed in tension.

3.1.3. Damage of bond

The bond between the steel plate and the concrete segment has two interfaces, namely the interface between the steel plate and the new concrete and the one between the new and the old concrete. In the test, radial stripping of the bond between the new and the old concrete is dominating. Its distribution is shown in Fig. 9. A comparison of the bond damages in the two strengthening schemes, as shown in Fig. 10, will be further discussed in Section 4.

Radial stripping occurred in the region from 320° to 28° and in the one from 165° to 230°. The maximum value of stripping occurred at 8°. Its value was 47.69 mm. The failure mode of the bond shows that the adhesive anchors were pulled out from the concrete segment without failing in tension. No tangential slippage was observed in the test.

3.2. Failure mechanism

The failure process of the strengthened structure under initial strengthening, tested in this study, was explained earlier in this section. The failure process of the strengthened structure under delayed strengthening was reported in previous research work [13], where six categories of cross-sections of the strengthened structure were defined. As regards the initial strengthening scheme, three situations are defined: situation 1, where the inner side of the cross-section is in tension and the outer side is in compression; situation 2, where the inner side of the cross-section is in compression and the outer side is in tension; and

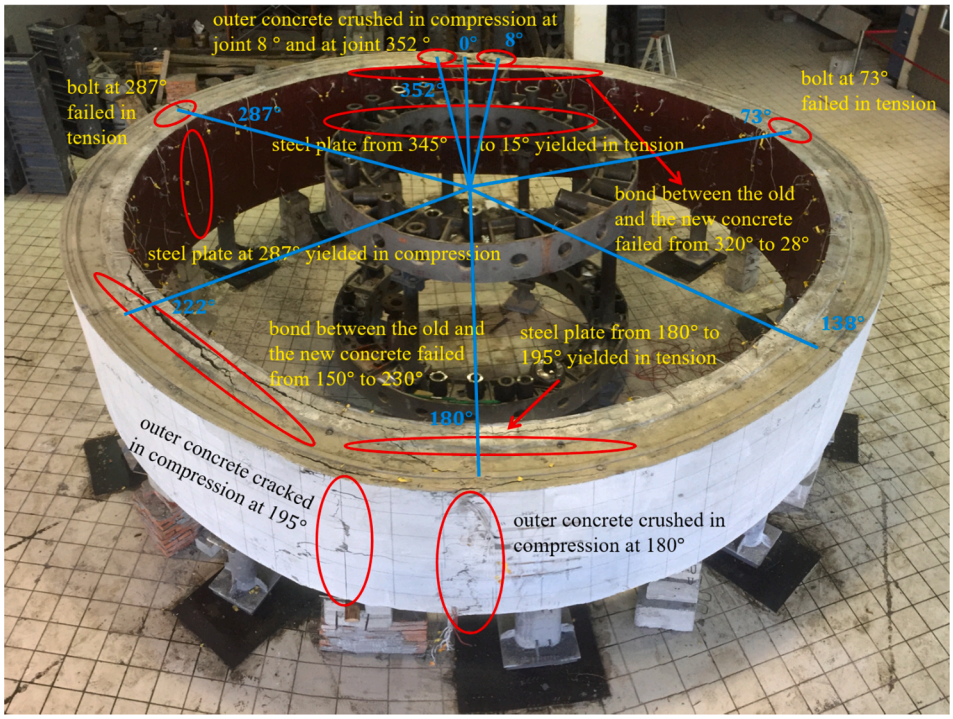

Fig. 6. Failure state of the segmental tunnel lining, strengthened by SPCCS before the start of loading.

situation 3, where both the inner and the outer side of the cross-section are in compression. The six categories are: (a) composite segment in situation 1; (b) composite segment in situation 2; (c) composite joint in situation 1; (d) composite joint in situation 2; (e) composite segment in situation 3; and (f) composite joint in situation 3. When the materials fails either in compression or in tension, the stiffness of the cross-section decreases rapidly, resulting in a plastic hinge.

The failure mechanism of the segmental tunnel lining, initially strengthened by SPCCS, is characterized by elasto-plastic deformations. The failure process is divided into the elastic range, the elasto-plastic range, and the plastic range. At P1 = 505 kN, tensile cracks occurred on the outer surface of the structure, which entered into the elasto-plastic range. This load level represents the elastic limit. At P1 = 788 kN, the bolt at joint 287° yielded. Hence, material in the tensile zone of the cross-section, belonging to category (d), was lacking. This resulted in the first plastic hinge. At P1 = 790 kN, the bolt at joint 73° yielded, resulting in the second plastic hinge. At P1 = 809kN, the outer concrete crushed at joint 8°, which belongs to category (c) of cross-sections. Material in the compressive zone was lacking. This resulted in the third plastic hinge. At P1 = 812 kN, the steel of the plate and of the reinforcement at the cross-section 180°, belonging to category (a), was yielding. This led to the fourth plastic hinge. Originally, the strengthened structure was statically indeterminate to the third degree. Thus, a kinematic chain developed at this load level, and the structure entered into the plastic range. This load level represents the bearing capacity limit. The structure was able to carry a slightly higher load instead of collapsing immediately, because it was surrounded by the horizontal loading system that provided support. However, the deformations increased rapidly and several parts of the steel plate yielded. The structure failed right after the outer concrete at 180° and 195° crushed. The vertical convergence reached 109 mm. The failure mechanism of the two tests will be compared in Section 4.1.

3.3. Structural deformations

The deformations of the structure in case of initial strengthening at the elastic limit and at the bearing capacity limit are shown in Fig. 11. The deformations at the bearing capacity limit in the test with delayed strengthening are also shown in Fig. 11. The cross-section of the deformed structure is similar to a transverse ellipse. The top and the bottom of the structure deform inwards, whereas the stopes deform outwards. In the test with initial strengthening, the vertical and the horizontal convergence at the elastic limit (P1 = 505 kN) were 6.33 mm and 4.48 mm, respectively. At the bearing capacity limit, i.e. at P1 = 812 kN, the vertical and the horizontal convergence were 99.03 mm and 92.42 mm, respectively. However, in the test with delayed strengthening, the vertical and the horizontal convergences, at the bearing capacity limit, i.e. at P1 = 768 kN, were 190.03 mm and 150.57 mm, respectively.

3.4. Opening of joints and bolt strain

The inner joint of the strengthened structure was covered by the strengthening material. Hence, only the dilations at the outer joints were measured. Load – joint opening diagrams are shown in Fig. 12, where positive values indicate the closure of the joint, whereas negative values signaled its opening. Before the elastic limit (P1 = 505 kN) is reached, openings and closures of joints are very small. The decrease of the joint stiffness is the consequence of yielding of the bolts at joints 73° and 287°, when P1 reached 790 kN, and of crushing of the concrete at 8°, for P1 = 809 kN.

As shown in Fig. 13, the bolt strains are small before the elastic limit is reached. This means that the neutral axis is at the location of the bolt. As the load increases, the bolt strains at joints 73° and 287° are in the elasto-plastic range.

Load – joint opening diagrams of joints subjected to a combination of axial forces and positive bending moments, as is the case at 8° and 352°, and to a combination of axial force and negative bending moment, as is the case at 73° and 287°, are compared separately, see Fig. 14. The results from the two strengthening schemes will be compared and discussed in Section 4.

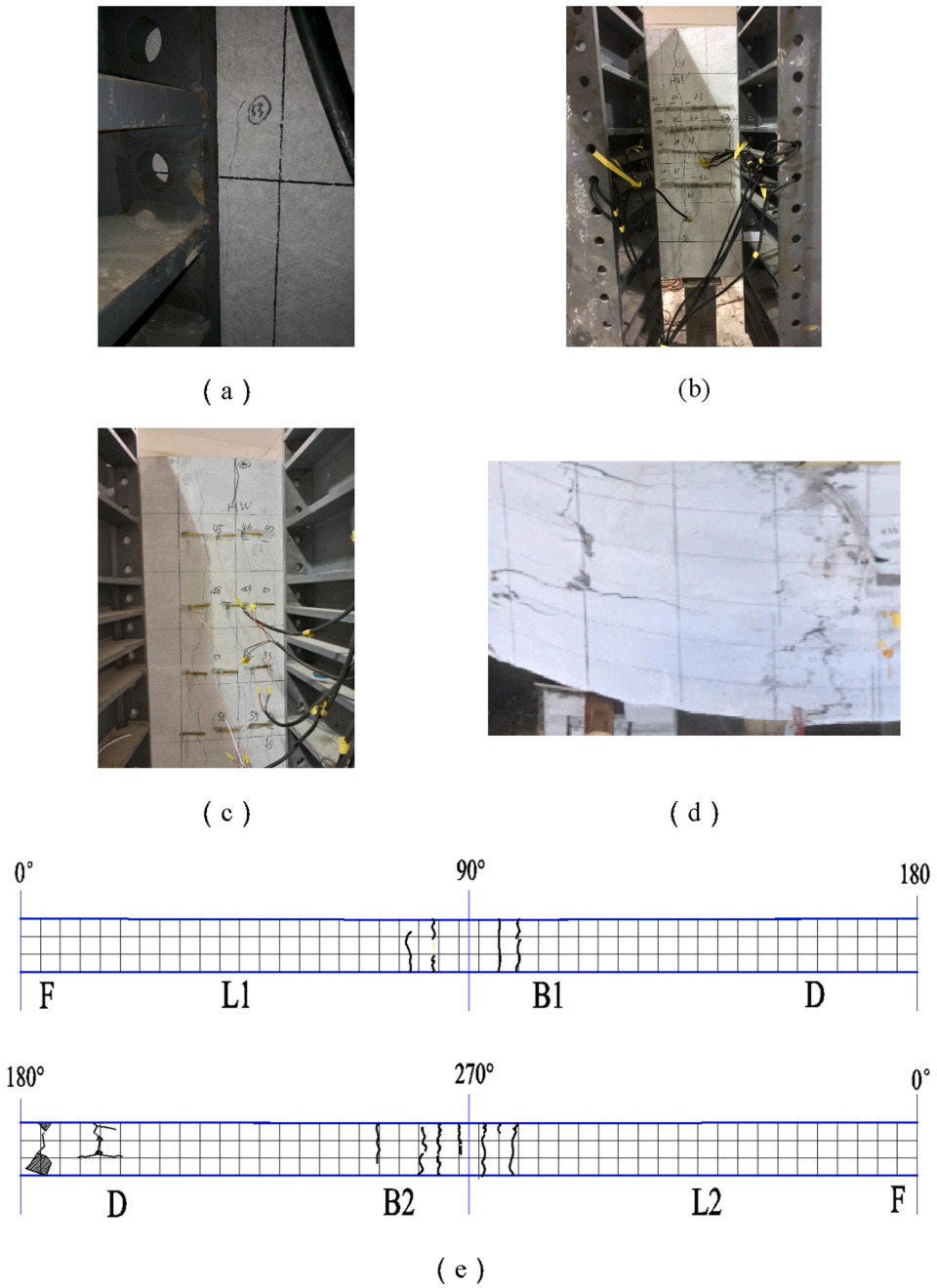

Fig. 7. Segment failure: (a) first crack at 270°; (b) cracks at 90°; (c) cracks at 270°; (d) concrete failure at 180° and 195°; (e) region of segment failure.

3.5. Stress of the steel plate

The stress distribution in the steel plate at the ultimate capacity stage is shown in Fig. 15(a). The bearing capacity limit, recorded in the test of the initially strengthened structure, occurred at P1 = 812 kN. In the test of the structure with delayed strengthening, this was the case at P1 = 768 kN. The tensile stress refers to the inner circle and the compressive stress to the outer circle of the cross-section of the lining. In both tests, the yield stress, obtained as 238.22 MPa, was reached in the region from 345° to 15° and at 180°. The maximum compressive stresses occurred at joints 73° and 287°. They were smaller than the yield stress.

It is noteworthy that the yielded area in case of initial strengthening is much larger, and that the stress at 287° is close to the yield stress. The utilization efficiency of the strengthening material is defined as the ratio of the stress of the steel plate and its yield strength. Fig. 15(b) shows the utilization efficiency of the steel plate for both strengthening schemes. It is seen that the material is used much better in case of initial strengthening than in case of delayed strengthening.

3.6. Relative slippage and stripping value of the bond

There are two interfaces of the bond between the steel plate and the segmental tunnel lining, namely, the interface between the steel plate and the new concrete (denoted as SP-NC) and the one between the new and the old concrete (denoted as NC-OC). The tangential slippage and the radial stripping of both interfaces were measured in the test. The distributions of slippage and stripping values at the bearing capacity limit in case of delayed strengthening (S) and of initial strengthening (F) are shown in Fig. 16. Generally, slippage and stripping are not significant because of the high strength and ductility of the bond, achieved by a combination of studs, embedded steel bars, adhesive anchors, and steel-fiber reinforced concrete.

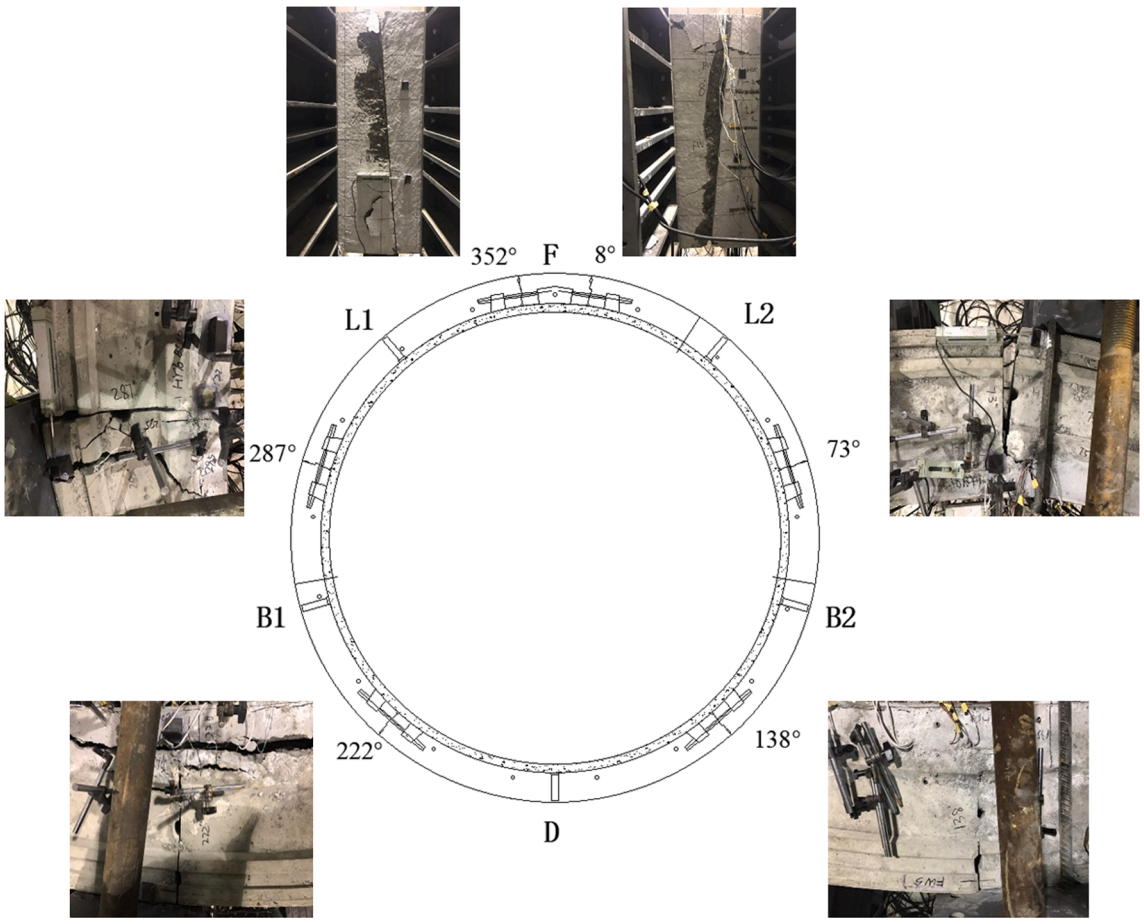

Fig. 8. Damage of joints at the failure state.

4. Comparison of the results with delayed strengthening

4.1. Structural state at failure

The failure state of the segmental tunnel lining, strengthened by SPCCS with a delayed strengthening scheme, was reported in detail in previous research [13]. In the following, the failure states in the tests with the two loading schemes will be compared:

1. The failure states in the two tests are similar. The cracks are distributed around 90° and 270°. The outer concrete crushes at two joints at the top. Crushing of the concrete segment occurs at the bottom. The steel plate yields in areas at the top as well as at the bottom.
2. The dominant mode of bond failure is radial stripping between the old and the new concrete. The failure mode is pull-out of the adhesive anchors. In both tests, the bond failures are distributed in regions with a combination of a positive bending moment and an axial force. The values of stripping in the test with initial strengthening are much larger than those in the test with delayed strengthening, as shown in Fig. 10.

In the delayed strengthening test, the bolts at joints 73° and 287° yield in tension, while failing in tension in the test with initial strengthening.

4.2. Failure mechanism

A comparison of load – vertical convergence diagrams of the structure, strengthened either initially or at the ultimate state, is shown in Fig. 17. Information on the failure process of the two strengthening schemes is shown in Table 3. The characteristic features ①–⑦ in case of initial strengthening are: ① strengthening of the structure, ② cracking of the outer concrete at 270°, ③ yielding of the bolt at joint 287°, resulting in the first plastic hinge, ④ yielding of the bolt at joint 73°, resulting in the second plastic hinge, ⑤ crushing of the outer concrete at joint 8°, resulting in the third plastic hinge, ⑥ yielding of the steel of the plate and the reinforcement at 180°, resulting in the fourth plastic hinge, and ⑦ failure of the structure. The characteristic features ①–⑥ in case of delayed strengthening are: ① strengthening of the structure, ② crushing of the outer concrete at joint 352°, resulting the first plastic hinge, ③ yielding of the bolt at joint 73°, resulting in the second plastic hinge, ④ crushing of the outer concrete at joint 8°, resulting in the third plastic hinge, ⑤ yielding of the steel of the plate and the reinforcement at 180°, resulting in the fourth plastic hinge, and ⑥ failure of the structure.

The failure mechanism of the structure, reinforced by the SPCCS strengthening technique, either by initial strengthening or by delayed strengthening, is characterized by a high degree of ductility. The failure process starts in the elastic range and is continued in the elasto-plastic and the plastic range. It is the bond, resulting from a combination of connectors and new concrete of high strength and ductility, that renders the strengthening material working together effectively with the original structure. Four plastic hinges develop in the elasto-plastic range, and a kinematic chain develops in the strengthened structure, noting that the structure is originally statically indeterminate to the third degree. Most of the plastic hinges occur at the segmental joints.

The main difference between the mechanical behavior of the two strengthened structures is that the length of the elasto-plastic range of the initially strengthened structure, which is 93 mm, is larger than the

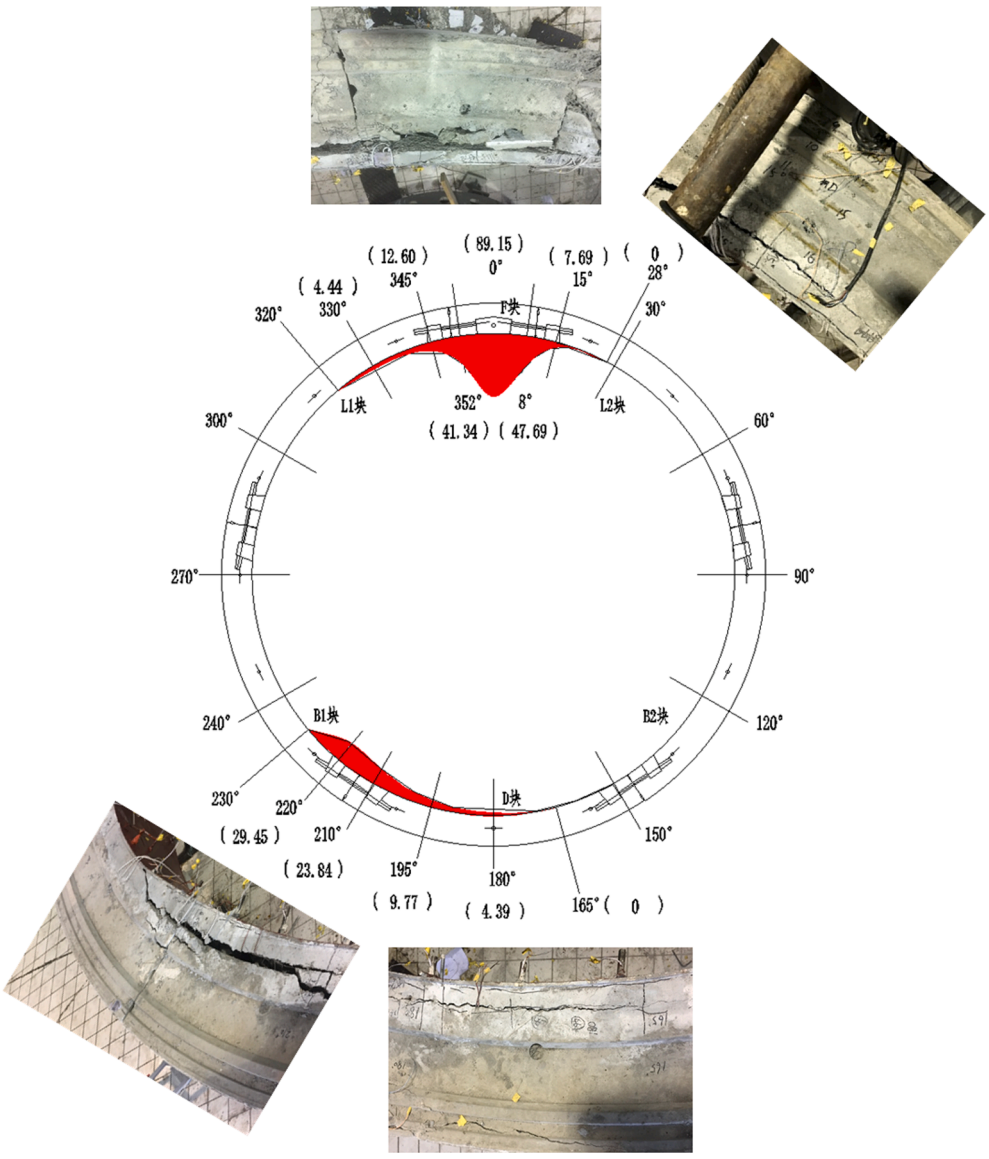

Fig. 9. Damage of bond at the failure state (unit: mm).

one of the structure characterized by delayed strengthening, namely, 48 mm. In other words, the latter enters into the plastic range faster than the former after having reached the elastic limit. Reasons for this situation are as follows: In case of initial strengthening, the elasto-plastic range starts when the outer concrete cracks in tension. At that instant of time, the stresses in all materials are still small. However, in case of delayed strengthening, the structure is strengthened when the tunnel lining is at the ultimate state, characterized by large stresses, especially in the outer concrete at joints 8° and 352° and in the bolts at joints 73° and 287°. Although the structure regains stiffness after strengthening, the strengthening material is only added to the inner surface, which contributes little to releasing the stresses of the outer concrete at joints 8° and 352° and of the bolts at joints 73° and 287°. Thus, the strengthened structure enters into the elasto-plastic range at a high stress level. Consequently, plastic hinges occur earlier than in case of initial strengthening. The length of the elasto-plastic range is only 51.7 % of the one in case of initial strengthening.

4.3. Ultimate capacity and overall stiffness

The load level and the vertical convergence of the structure at the strengthening point are denoted as P_0 and y_0, respectively. By analogy, the load level and the vertical convergence of the structure at the elastic limit are denoted as P_e and y_e, respectively. By analogy, P_u and y_u refer to the bearing capacity limit. The slope of the lines ①–② in Fig. 17 represents the stiffness of the strengthened structures. It is denoted as k_e. Table 4 contains a comparison of the ultimate capacity and the structural stiffness for the two strengthening schemes.

In case of initial strengthening, the ultimate capacity is 812 kN, whereas the structural stiffness is 79.773 kN/mm. In case of delayed strengthening, the ultimate capacity is 768 kN, while the structural stiffness is 12.854 kN/mm. The ultimate capacity in case of initial strengthening is 5.7 % larger than that for delayed strengthening. As regards the structural stiffness, this quantity is by 520.6 % larger for initial strengthening than for delayed strengthening.

The influence of the timing of strengthening on the ultimate capacity is very small. This is because the distribution of the internal forces is only slightly influenced by the deformations of a circular structure. The ultimate capacity is determined by the fourth plastic hinge at 180°, where the steel of the plate and the reinforcement yields in tension and the outer concrete crushes. Hence, when the fourth plastic hinge occurs, both the distributions of the internal forces from the two tests and the

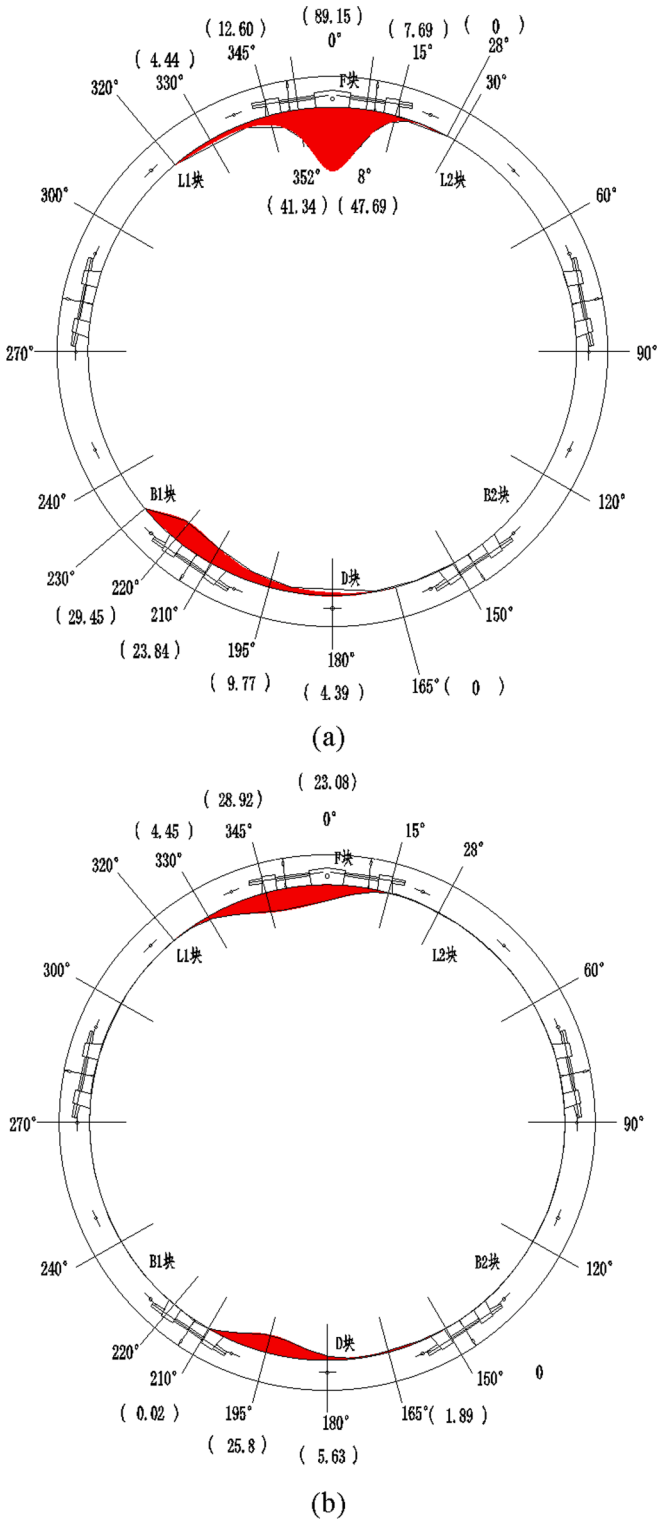

Fig. 10. Radial stripping of the interface between the old and the new concrete for the case of (a) initial strengthening and (b) delayed strengthening of the tunnel segment.

external loads are similar. However, the timing of strengthening has a significant influence on the structural stiffness. The reason for this is that the structural deformations are mainly caused by the relative rotations of the segmental joints. Their behavior is influenced by the timing of strengthening.

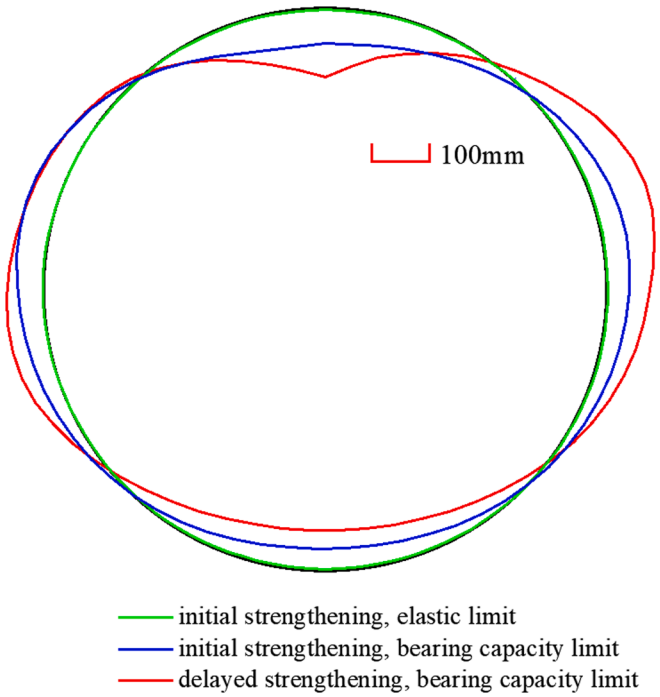

Fig. 11. Structural deformations for the two strengthening schemes.

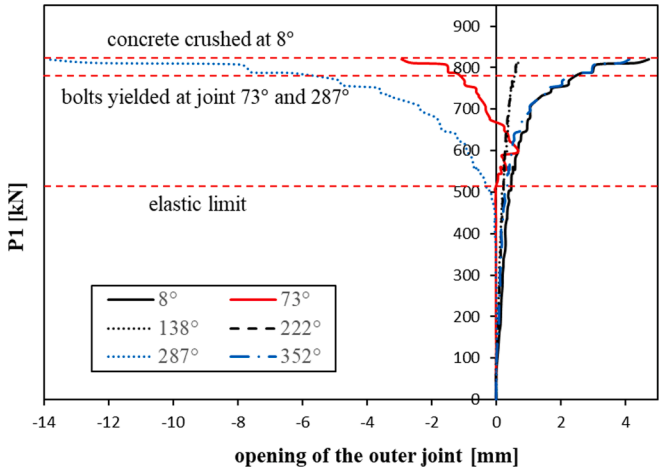

Fig. 12. Load- joint opening diagrams from the test with initial strengthening.

4.4. Joint deformation

The dilations of joints are an important factor contributing to the structural deformation. Therefore, they should be compared and discussed. Fig. 14 contains a comparison of the opening of joints for different strengthening timings.

Regarding joints 8° and 352°, the outer part is in compression and the inner part in tension. In the elastic range, the stiffness of joint 8° for the case of delayed strengthening is close to the one for initial strengthening, whereas the stiffness of joint 352° for delayed strengthening is significantly smaller than the one for initial strengthening. This has happened because, in the test with delayed strengthening, the elastic range of the strengthened structure starts at the strengthening point, at which the structure is already deformed. The outer concrete at joint 352° has cracked in compression, reducing the area of the compressive zone. Although the height of the cross-section is increased and the neutral axis is lowered towards the tensile zone in consequence of the addition of strengthening material to the inner surface of the lining, the increase of

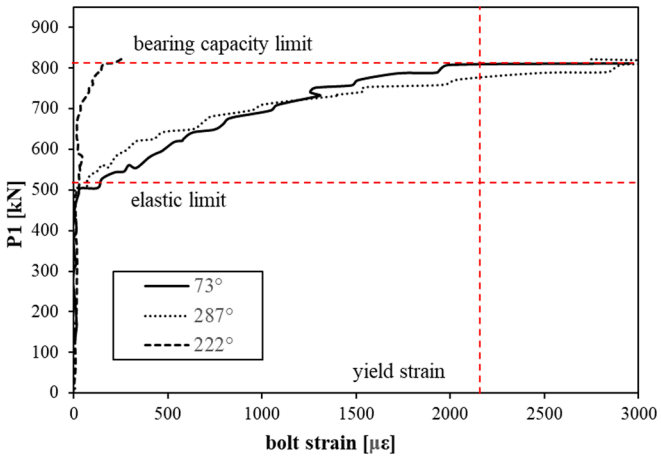

Fig. 13. Load – bolt strain diagrams from the test with initial strengthening.

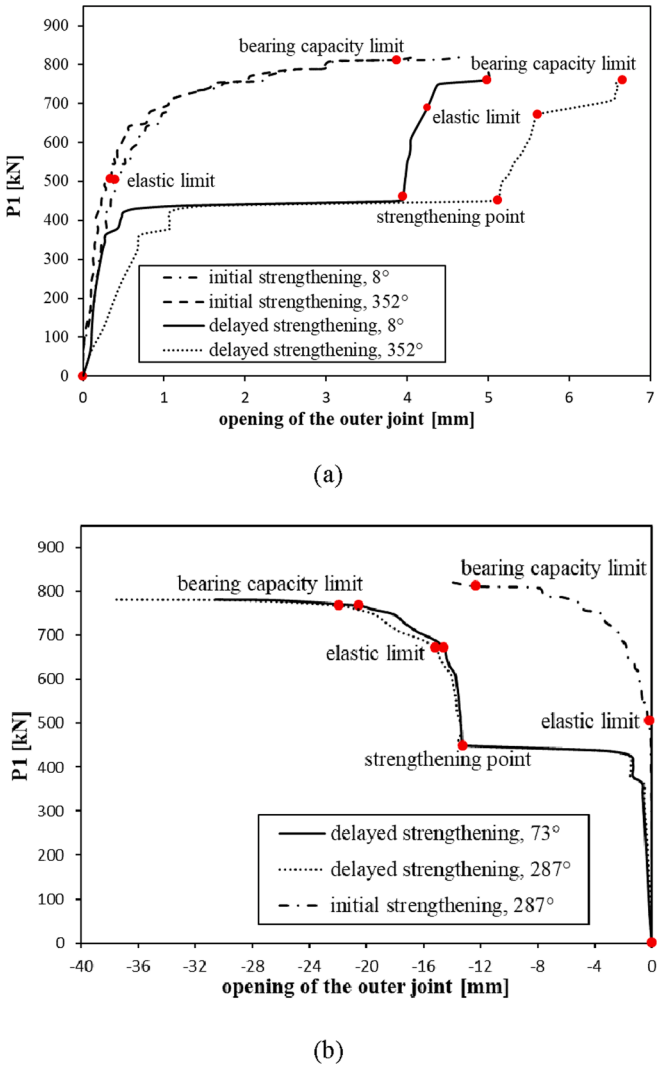

Fig. 14. Comparison of load – joint opening diagrams for joints subjected to (a) a positive bending moment and (b) a negative bending moment.

the joint stiffness is limited. However, the outer concrete at joint 8° remains undamaged, and the area of the compressive zone is the same as the one in the initially strengthened structure. In the elasto-plastic range, the stiffness of both joints is small for both modes of strengthening, because the concrete in the compressive zone has crushed, resulting in a reduction of the area of the compressive zone.

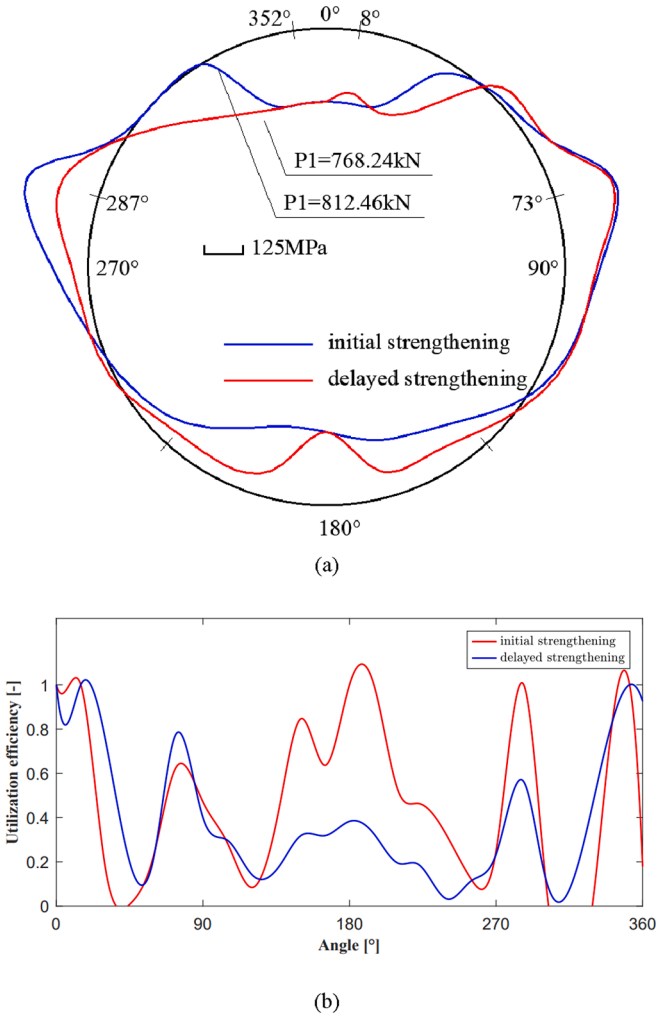

Fig. 15. (a) Stress distribution and (b) utilization efficiency of the steel plate for the two strengthening schemes at the ultimate capacity stage.

Regarding joints 73° and 287°, the outer part is in tension, whereas the inner part is in compression. The stiffness of the joints in the elastic range in case of initial strengthening of the segmental tunnel ring is much larger than that in case of delayed strengthening. The reason for this is that the segmental joints represent discontinuities of the structure. In case of delayed strengthening, at the strengthening point, the steel of the bolts is the only material providing tensile resistance. The strengthened structure is tested in a situation where the neutral axis of the cross-section is very close to its outer part. Thus, the area of the compressive zone is small. However, in case of initial strengthening, the neutral axis is very close to the centroidal axis of the cross-section at the beginning of the test. The area of the compressive zone is significantly larger than the one in case of delayed strengthening, and the joint stiffness is much larger. In the elasto-plastic range, the joint stiffness is similar for the two modes of strengthening. In summary, the joint stiffness is significantly influenced by the strain state of the cross-sections of the joints before strengthening.

4.5. Ductility

The structural ductility, μ_c, is an important indicator in engineering. It is defined as.

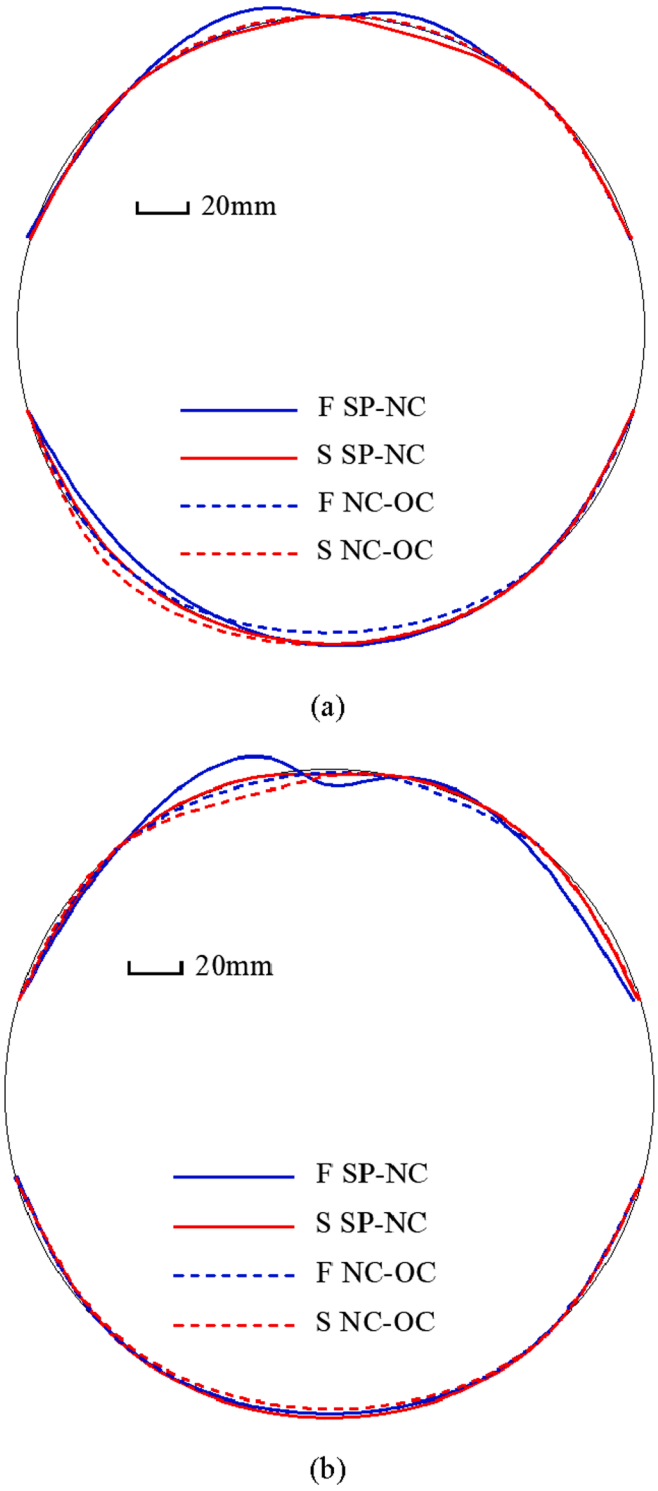

Fig. 16. Distribution of (a) slippage and (b) stripping of the interfaces between the steel plate and the new concrete and between the new concrete and the old concrete, at the bearing capacity limit.

$$\mu_c = \frac{y_u - y_0}{y_1 - y_0}, \tag{1}$$

where y_1 is the vertical convergence at the yield point. y_0 and y_u were defined previously. The yield point is obtained by "the farthest-point method", proposed in previous research [5]. As shown in Fig. 18, the yield point A (y_1, P_1) is the point on the load – vertical convergence diagram with the largest distance from the line connecting the strengthening point B (y_0, P_0) and point C (y_u, P_u). The coordinate of point A is calculated as follows: At first, the distance from the alternative point D(y_i, P_i) on the load – vertical convergence diagram to the line BC is calculated by.

$$d_i = \frac{\left|(P_u - P_0)(y_i - y_0) - (y_u - y_0)(P_i - P_0)\right|}{\sqrt{(y_u - y_0)^2 + (P_u - P_0)^2}}. \tag{2}$$

Then, the maximum value of d_i is computed. The respective coordinate defines the location of the yield point A. It follows from.

$$(y_1, P_1) = \max_{(y_1,P_1)=(y,P)} \frac{\left|(P_u - P_0)(y - y_0) - (y_u - y_0)(P - P_0)\right|}{\sqrt{(y_u - y_0)^2 + (P_u - P_0)^2}}. \tag{3}$$

As mentioned previously, most of the plastic hinges occur at the segmental joints. Hence, their ductility, μ_j, is an important indicator of the structural behavior. Based on the data in Fig. 14, μ_j can be calculated

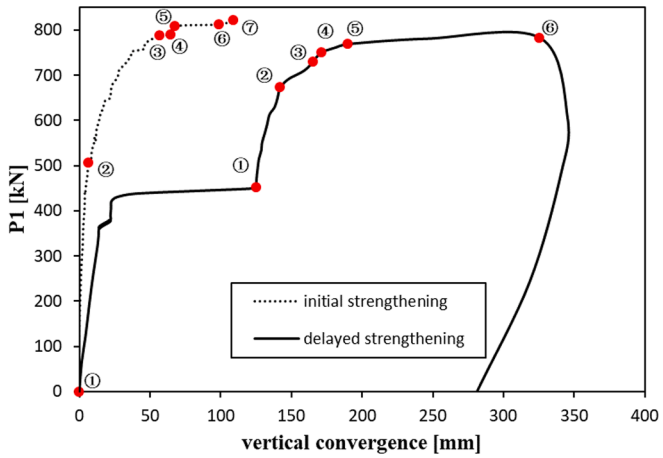

Fig. 17. Comparison of load – vertical convergence diagrams obtained from tests concerning the two modes of strengthening.

Table 3
Information on the failure process of the two strengthening schemes.

	Initial strengthening			Delayed strengthening		
	No.	P1 [kN]	Vertical convergence [mm]	No.	P1 [kN]	Vertical convergence [mm]
Strengthening point	①	0	0	①	452	125
Elastic limit	②	505	6	②	672	142
Elastio-plastic stage	③	785	57	③	730	166
	④	790	65			
	⑤	809	68	④	751	172
Bearing capacity limit	⑥	812	99	⑤	768	190
Plastic stage	⑦	821	109	⑥	782	325

Table 4
Comparison of the ultimate capacity and the structural stiffness for the two strengthening schemes.

Index	Initial strengthening	Delayed strengthening
P_0 (kN)	0	451
y_0 (mm)	0	125
P_e (kN)	505	672
y_e (mm)	6	142
P_u (kN)	812	768
y_u (mm)	99	190
k_e(kN/mm)	80	13

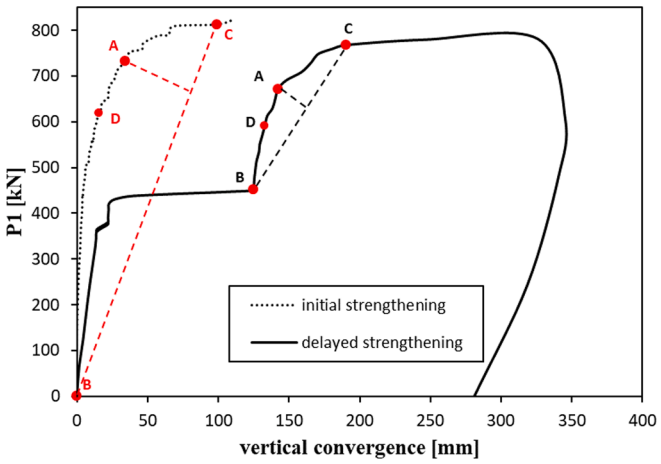

Fig. 18. On the definition of the yield point.

as:

$$\mu_j = \frac{d_u - d_0}{d_1 - d_0}, \tag{4}$$

where d_o, d_1, and d_u are the values of opening of the outer joint at the strengthening point, the yield point, and at the bearing capacity limit, respectively. With the help of the "farthest-point method", the yield point is obtained as.

$$(d_1, P_{j1}) = \max_{(d_1,P_{j1})=(d,P_j)} \frac{\left|(P_{ju} - P_{j0})(d - d_0) - (d_u - d_0)(P_j - P_{j0})\right|}{\sqrt{(d_u - d_0)^2 + (P_{ju} - P_{j0})^2}}, \tag{5}$$

where P_{j0}, P_{j1}, and P_{ju} denote the load at the strengthening point, the yield point, and the bearing capacity limit, respectively.

Results for μ_c, μ_j^p, and μ_j^n are listed in Table 5. μ_c denotes the ductility of the structure. μ_j^p stands for the ductility of the segmental joint subjected to a positive bending moment and μ_j^n denotes the ductility of the segmental joint subjected to a negative bending moment. These three quantities are larger for the case of initial strengthening than the ones for the case of delayed strengthening, obtained as 46.1 %, 423.3 %, and 25.0 %. Thus, the timing of strengthening has a significant influence on the ductility of strengthened structures. Its influence on segmental joints subjected to positive bending moments is much larger than the one on segmental joints subjected to negative bending moments.

4.6. Toughness

Toughness denotes the ability of a structure to absorb energy and to deform plastically without fracturing. In the Japanese standard [7], toughness is defined as the mechanical energy that a beam can absorb when its deformation reaches L/150, where L denotes the span of the beam. However, so far there is no definition of the toughness of segmental tunnel linings. Considering that the existence of segmental joints increases the ability of the structure to deform, the toughness, E, is defined as the mechanical energy that the structure can absorb between the strengthening point and the bearing capacity limit [12], have introduced the calculation of E in previous research.

In the full scale test, described in this paper, the structure was subjected to 24 point loads, P_i, directed to the center of the tunnel ring, as shown in Fig. 4(a). The radial displacement of each load point is denoted as D_i. If the displacement of the load point is directed inwards, D_i is assumed to be positive. The work done by the load P_i is given as.

$$E_i = \int P_i dD_i. \tag{6}$$

It is equal to the shaded area in Fig. 19. The total mechanical energy of the structure is obtained as,

$$E = \sum_{i=1}^{24} \int P_i dD_i \tag{7}$$

As shown in Fig. 4(a), there are 24 load points. However, only 14 measurement points are deployed. Hence, the displacements of some load points are unknown. Herein, Catmull-Rom splines are employed to draw the overall deformation configuration of the structure, based on data obtained from 14 measurement points. Then, the displacements of 24 load-points can be determined and E can be calculated. The value of E for the case of initial strengthening and the one of delayed strengthening is 134.40 kJ and 81.66 kJ, respectively. Thus, the toughness of the initially strengthened structure is by 64.6 % larger than the one in case of delayed strengthening.

Table 5
Ductility for the two strengthening schemes.

Indices	Initial strengthening	Delayed strengthening
μ_c	5.55	3.80
μ_j^p	5.39	1.03
μ_j^n	6.65	5.32

5. Conclusions

The following conclusions are drawn from the experimental investigation described in this paper:

1. The SPCCS strengthening technique results in a significant increase of the bearing capacity and of the stiffness of segmental tunnel linings. This follows from the strong bond between the steel plate and the concrete segments, caused by a combination of struts, embedded steel bars, adhesive anchors, and steel-fiber reinforced concrete. This kind of bond results in particularly high strength and ductility. It allows the steel plate to work together with the segmental tunnel lining during the whole loading process.
2. The failure mechanism of the strengthened structure is hardly influenced by the timing of strengthening. It is characterized by a high degree of ductility. Four plastic hinges were noticed when the structure reached the limit of the bearing capacity. It is noteworthy that the plastic hinges are predominantly located at the segmental joints.
3. Timing of the strengthening has little influence on the bond behavior in case of the SPCCS strengthening technique. However, the efficiency of the action of the steel plate is influenced by this timing.

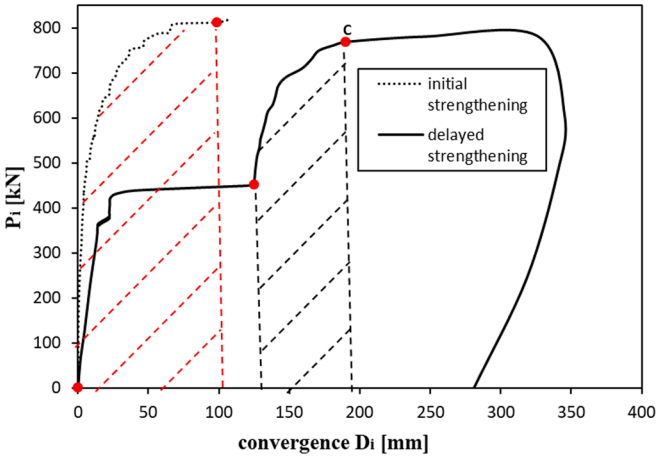

Fig. 19. On the calculation of the mechanical energy.

4. The segmental joints are the weakest parts of the strengthened structure. Their stiffness is significantly influenced by the timing of strengthening. If the structure is strengthened earlier, the stiffness and the ductility of the strengthened joint will be higher.
5. The timing of strengthening has only little influence on the ultimate capacity. The ultimate capacity of the strengthened structure in case of initial strengthening is only 5.7 % larger than the one in case of delayed strengthening.
6. The timing of strengthening has a significant influence on the stiffness, the ductility, and the toughness of the strengthened structure. For the initially strengthened structure, these three quantities are by 520.6 %, 46.1 %, and 64.6 % larger than the respective quantities of the structure with delayed strengthening.
7. If the ultimate capacity of the structure is a critical factor, the timing of strengthening is not an important parameter. However, if the structural serviceability is a decisive factor, the earlier the structure is strengthened, the better its serviceability will be.

In this paper, a detailed comparison of the mechanical performance of structures, strengthened at extreme instants of time of strengthening was presented. This comparison was based on experimental data. One structure was strengthened before the start of the loading process (*ab initio* strengthening). The other one was strengthened when the structure reached its ultimate state (delayed strengthening). However, in real-world engineering projects, the structure is strengthened between these two extreme instants of time. Therefore, a model for prediction of the structural behavior for different instants of strengthening would be useful. The experimental data and the results obtained in this research provide the basis for such a model.

Declaration of Competing Interest

The authors declare that they have no known competing financial interests or personal relationships that could have appeared to influence the work reported in this paper.

Data availability

Data will be made available on request.

Acknowledgement

This research was financially supported by the National Natural Science Foundation of China (Grant No. 52078376, 52038008) and the State Key Laboratory for Hazard Reduction in Civil Engineering of Tongji University (Grant No. SLDRCE19-B-39). The authors acknowledge TU Wien Bibliothek for financial support through its Open Access Funding Programme.

References

[1] Avanaki MJ. Effects of hybrid steel fiber reinforced composites on structural performance of segmental linings subjected to TBM jacks. Struct Concr 2019;6:1909–25.
[2] Blom CBM. Design philosophy of concrete linings for tunnels in soft soils. Delft, The Netherlands: Delft University of Technology; 2002. Ph.D. Dissertation.
[3] Bursi OS, Gramola G. Behaviour of composite substructures with full and partial shear connection under quasi-static cyclic and pseudo-dynamic displacements. Mater Struct 2000;33(227):154–63.
[4] Chang CT, Sun CW, Duann SW, Hwang RN. Response of a Taipei Rapid Transit System (TRTS) tunnel to adjacent excavation. Tunn Undergr Space Technol 2001;16(3):151–8.
[5] Feng P, Qiang HL, Ye LP. Discussion and definition on yield points of materials, members and structures. Eng Mech 2017;34(3):36–46.
[6] Gong W, Juang CH, Huang H, Jia Z, Zhe L. Improved analytical model for circumferential behavior of jointed shield tunnels considering the longitudinal differential settlement. Tunn Undergr Space Technol 2015;45:153–65.
[7] JSCE Standard-SF4. Method of tests for flexural strength and flexural toughness of steel fiber reinforced concrete. JSCE Jpn Soc Civ Eng 1984;3:58–61.
[8] Kiriyama K, Kakizaki M, Takabayashi T, Hirosawa N, Imafuku K. Structure and construction examples of tunnel reinforcement method using thin steel panels. Nippon Steel Tech Rep 2005;92:45–50.
[9] Li X, Lin X, Zhu H, Liu Z. Condition assessment of shield tunnel using a new indicator: the tunnel serviceability index. Tunn Undergr Space Technol 2017;67:98–106.
[10] Liu X, Jiang Z, Zhang L. Experimental investigation of the ultimate bearing capacity of deformed segmental tunnel linings strengthened by epoxy-bonded filament wound profiles. Struct Infrastruct Eng 2017;13(10):1268–83.
[11] Liu X, Jiang Z, Yuan Y, Mang HA. Experimental investigation of the ultimate bearing capacity of deformed segmental tunnel linings strengthened by epoxy-bonded steel plates. Struct Infrastruct Eng 2018;14(6):685–700.
[12] Liu X, Jiang Z, Yuan Y, Mang HA. Numerical investigation of the mechanical behavior of deformed segmental tunnel linings, strengthened by epoxy-bonded filament wound profiles. Tunn Undergr Space Technol 2018;78:231–44.
[13] Liu X, Jiang Z, Mang HA. Experimental investigation of the bearing capacity of deformed segmental tunnel linings strengthened by a special composite structure. Struct Infrastruct Eng 2021. doi: 10.1080/15732479.2021.1924796.
[14] Nakamura H, Kubota T, Furukawa M, Nakao T. Unified construction of running track tunnel and crossover tunnel for subway by rectangular shape double track cross-section shield machine. Tunn Undergr Space Technol 2003;18(2–3):253–62.
[15] Nakashima M, Matsumiya T, Suita K. Full-scale test of composite frame under large cyclic loading. J Struct Eng 2007;133(2):297–304.
[16] Nie J, Fan J, Cai CS. Experimental study on flexural behavior of composite beams with different concrete flange construction. J Struct Eng 2004;130(11):1842–51.
[17] Nie J, Xiao Y, Chen L. Experimental studies on shear strength of steel–concrete composite beams. J Struct Eng 2004;130(8):1206–13.
[18] Nie J, Tang L, Cai CS. Performance of steel-concrete composite beams under combined bending and torsion. J Struct Eng 2009;135(9):1048–57.
[19] Nie J, Li F, Fan J, Zhang X, Diao S. Experimental study on flexural behavior of composite beams with different concrete flange construction. J Highway Transport Res Dev 2011;5(1):30–5.
[20] Nie J, Tao M, Cai CS, Ge C. Modeling and investigation of elasto-plastic behavior of steel–concrete composite frame systems. J Constr Steel Res 2011;67(12):1973–84.
[21] Schreyer J, Winselman D. Suitability tests for the lining for the 4th Elbe Tunnel Tube - results of large-scale tests. Tunnel 2000;1:33–44.
[22] Yuan Y, Jiang X, Liu X. Predictive maintenance of shield tunnels. Tunn Undergr Space Technol 2013;38:69–86.